THE ASTROPHYSICAL JOURNAL, 414:154–164, 1993 September 1

THRESHOLD STAR-FORMATION EFFECTS IN THE PECULIAR GALAXY ARP 10 (=VV 362)

V. CHARMANDARIS AND P. N. APPLETON[1]
Department of Physics and Astronomy, Iowa State University, Ames, IA 50011
AND
A. P. MARSTON[1]
Department of Physics and Astronomy, Drake University, Des Moines, IA 50311
Received 1992 October 16; accepted 1993 March 12

ABSTRACT

We present images of the peculiar galaxy Arp 10 which reveal two rings of concurrent star formation. Apart from a bright ring visible on early photographs of the system, an even brighter inner ring of H II regions is found within the nuclear bulge of the galaxy. A very faint ring-arc of H II regions is also seen associated with a third outer ring or shell. We detect a small companion galaxy on the minor axis of Arp 10 and an extended extra-nuclear knot which lies between the first and second rings. An investigation of the Hα fluxes in the rings reveals an increase in the emission where the ring surface density in the *R*-band light exceeds 21.3 ± 0.2 mag arcsec^{-2}. If the *R*-band light is dominated by old stars in the underlying density wave, then the results suggest evidence for a star-formation law which exhibits a threshold dependence on the strength of the density wave in the rings. Even if the *R*-band continuum in the ring is heavily contaminated with red light from the underlying young stars (a result at odds with the smooth continuum morphology of the ring) then a smaller, but still significant nonlinear enhancement in the star-formation rates in one segment of the second ring is required to explain the results. In either case, strong trends in the star-formation rate with azimuth around Ring 2 are in good agreement with off-center collisional ring galaxy models.

Subject headings: galaxies: individual (Arp 10) — galaxies: stellar content — stars: formation

1. INTRODUCTION

Arp 10 (=VV 362) is a galaxy containing a bright ring, an off-center nucleus and a faint bar. Vorontsov-Velyaminov (1977) describes the galaxy as containing "... an enormously developed massive part of the ring" which we will later show is a region of enhanced star formation in the ring. Arp 10 was noted as a ring galaxy by Dahari (1985). Faint traces of outer filaments resembling antennae are seen protruding from the galaxy in the photograph presented in the Arp Atlas of Peculiar Galaxies (Arp 1966) suggesting that Arp 10 may be a colliding system. Although the outer filaments in Arp 10 in some ways resemble shells around some elliptical galaxies (Malin & Carter 1983), the single-dish H I spectrum of the galaxy obtained by Sulentic & Arp (1983) exhibits the typical two-horned profile of a rotating planar disk.

We present deep CCD images of Arp 10 which support the collisional picture for the formation of the ring and filaments. A small elliptical companion is found approximately one ring diameter from Arp 10 on its minor axis, suggesting that Arp 10 may be a ring galaxy formed by the head-on collision of a small intruder galaxy through the center of a rotating disk (Lynds & Toomre 1976; Theys & Spiegel 1977). Another ring and additional ring-arcs are also discovered in the light of Hα in Arp 10. The newly discovered ring lies in the inner regions of the central bulge. The Hα imaging also reveals sharply defined ring-arcs associated with the faint outer filaments. Multiple rings are expected in well evolved models of colliding ring galaxies (Toomre 1978; Appleton & Struck-Marcell 1987, hereafter ASM; Struck-Marcell 1990).

Ring galaxies provide an ideal laboratory for exploring models of star formation triggered by density waves. Of special interest is the mildly off-center collision between an intruder galaxy and a disk. It has been argued by Appleton & Struck-Marcell (1987) that such a collision will generate an expanding ring wave which shows large but smooth variation in stellar and gaseous density around the ring. Such a wave is an ideal tool for exploring the dependence of star-formation rate (hereafter SFR) on ring surface density in galaxies. The work is relevant to threshold star formation mechanisms such as those put forward by Scalo & Struck-Marcell (1984, 1986), Struck-Marcell & Appleton (1987, hereafter SMA), for colliding systems as well as Kennicutt (1989, 1990) for normal galaxies. (See also observations by Skillman 1987; Schombert & Bothun 1988; Carignan & Beaulieu 1989).

In this paper we will investigate the peculiar morphology of Arp 10 and will calculate the SFR in the bright knots in all three ring structures. In § 2 we describe our observations and we present the optical morphology of Arp 10 in § 3. In § 4 we present details of how we performed the photometry and the SFR calculations. The results are presented in § 5. In § 6 we describe some predictions based on existing models. In § 7 we discuss their physical significance, and our conclusions are highlighted in § 8. The systematic heliocentric velocity of Arp 10 is 9093 km s^{-1} (Sulentic & Arp 1983). Using the velocity corrected for motion relative to the local group (de Vaucouleurs, de Vaucouleurs, & Corwin 1976) and assuming a value for the Hubble constant of 75 km s^{-1} Mpc^{-1} we estimate a distance to Arp 10 of 122 Mpc.

2. OBSERVATIONS

The observations were made during photometric conditions on the night of 1991 January 19 using the KPNO 2.1 m tele-

[1] Visiting astronomer at the Kitt Peak National Observatory. KPNO is operated by the Association of Universities for Research in Astronomy, Inc., under contract with the National Science Foundation.

scope. Images were obtained through a broad-band R and a narrow-band 80 Å wide filter, centered close to the wavelength of redshifted Hα and [N II]. The detector was a Tek2 512 × 512 pixel^2 CCD. Two 1500 s observations were made using the Hα + [N II] filter in order to detect emission from the star-forming knots. A 1200 s exposure was taken using the R-band filter. Bias subtraction and flat-fielding of the images were performed in a standard way. Flat fields were obtained using sky observation made during the morning twilight. The continuum was removed from the spectral line images using a carefully scaled R-band image. The seeing disks were very similar for both the line and continuum images (FWHM = 1″.2). Calibration of the photometry was performed using data taken from the star Hz 15 (Stone 1977) and the standard star 95 52 (Landolt 1983).

As a further check of the reliability of the R-band image as a good representation of the stellar continuum, we made further observations of Arp 10 with the newly commissioned wide-field CCD system at Iowa State University's E. W. Fick Observatory. The Fick wide-field CCD camera was attached to the 0.6 m Mather telescope with a focal reducer providing an f/4 beam at the detector. The CCD is a thinned TI 800 × 800 pixel^2 device providing a 1″.3 pixel^{-1} image scale. The observations of Arp 10 were made during the nights of 1992 August 28 and 29 through a narrow band, 50 Å wide interference filter, centered at 6700 Å. This provided a narrow-band continuum with no possibility of contamination by hydrogen emission lines. No discernible difference was found between the KPNO R-band and the Fick Observatory image down to a level of 5% (see Appendix).

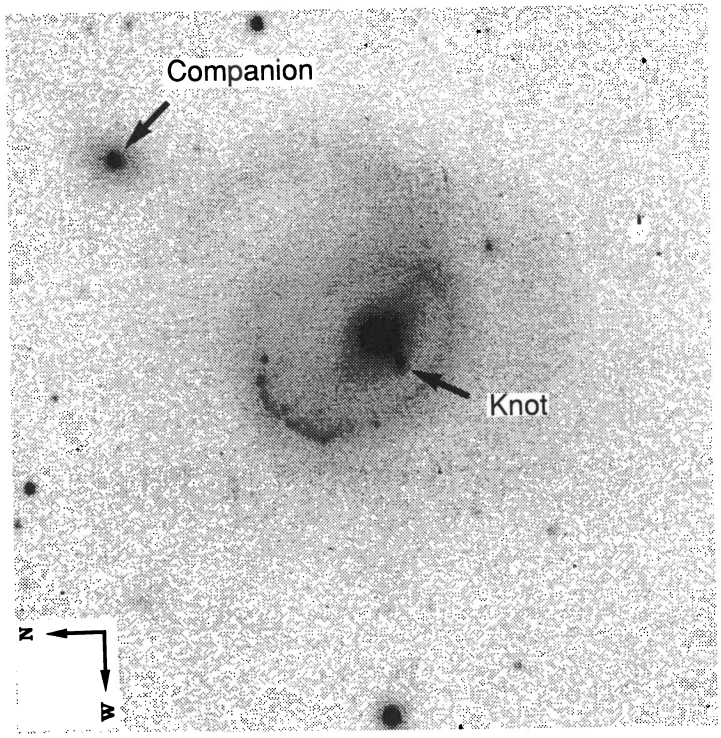

FIG. 1.—Gray-scale image of Arp 10 through the R-band filter. Note the possible elliptical companion galaxy seen to the northeast of Arp 10 and the bright extra-nuclear knot which lies to the west of the nucleus. North is to the left and west is at the bottom in all the images in this paper.

3. OPTICAL MORPHOLOGY

A gray-scale representation of the R-band image is shown in Figure 1. The galaxy has a dominant ring containing a nucleus and faint bar and an outer structure which extends from the south-east in shell-like filaments. We indicate in Figure 1 a possible elliptical companion galaxy to Arp 10, which lies 60″ to the northeast on the minor axis of the ring. If Arp 10 is a collisional ring system this is a prime candidate for the intruder galaxy. A bright extra-nuclear knot is also seen close to the nucleus of Arp 10 to the southwest. This knot, which is also marked in Figure 1, may be in some way related to the collisional nature of the system. It is also visible in Hα emission, which indicates that it must belong to the system. We will not elaborate more on its nature since we do not yet have radial velocity measurements which would help to further define its relationship to the disk of Arp 10.

In Figures 2 and 3 we show a gray-scale image and a contour map, of the Hα + [N II] line emission from Arp 10. In addition to the bright ring we also see for the first time the strong inner line-emitting ring which lies within the central bulge of Arp 10. Faint outer emission knots are also visible associated with the shell-like continuum especially to the northeast. We will refer to the inner ring, the bright intermediate ring and the outer ring-arcs (see Fig. 2) as Rings 1, 2 and Ring-arc 3 throughout this paper. The radii of the three ring-like structures are 2″.8, 21″.5, and 40″, respectively.

4. PHOTOMETRY AND SFR CALCULATIONS OF THE RING KNOTS AND ARCS

The photometric fluxes of the many bright knots in Arp 10 were determined in two ways:

I. We integrated the flux contained within each knot down to an Hα isophotal level of 0.60×10^{-16} ergs cm^{-2} s^{-1} arcsec^{-2} (2.5 × rms noise level in the image). The boundaries defined by this isophotal level in the Hα map were then transferred to the suitably registered R-band continuum image in order that the R-band flux be estimated over the same area. From these flux estimates and a knowledge of the area of the limiting contour, we then calculated the surface brightness of the regions in both Hα and red continuum light.

II. We performed photometry in a fixed circular software aperture with a radius of 2″.87 centered on each bright knot of Ring 2. Again the surface brightness at the same aperture center was estimated once the fluxes had been evaluated.

We calculated the surface brightness using these two different methods in order to ensure that the surface area of the flux evaluation did not play a significant role in the final results. Indeed, as will be shown below, the two methods yield similar results.

In Figure 2, we indicate the specific areas over which the flux was evaluated down to the isophotal limit given above (Method I). The regions, presented in Table 1, are labeled 1–29, for future reference. We note that for the very bright northwest region of Ring 2, an entire portion of the ring exceeds the isophotal limit because the many bright knots which lie close together in that region cause the contours to merge. Since we are primarily interested in surface brightness rather than total flux in our discussion below, we decided to split up this part of the ring into segments equal to the isophotal thickness of the ring (about 5″). We attempted to include one bright H II region complex in each ring segment and avoided bisecting bright partially resolved hot spots. A similar argument applies to the

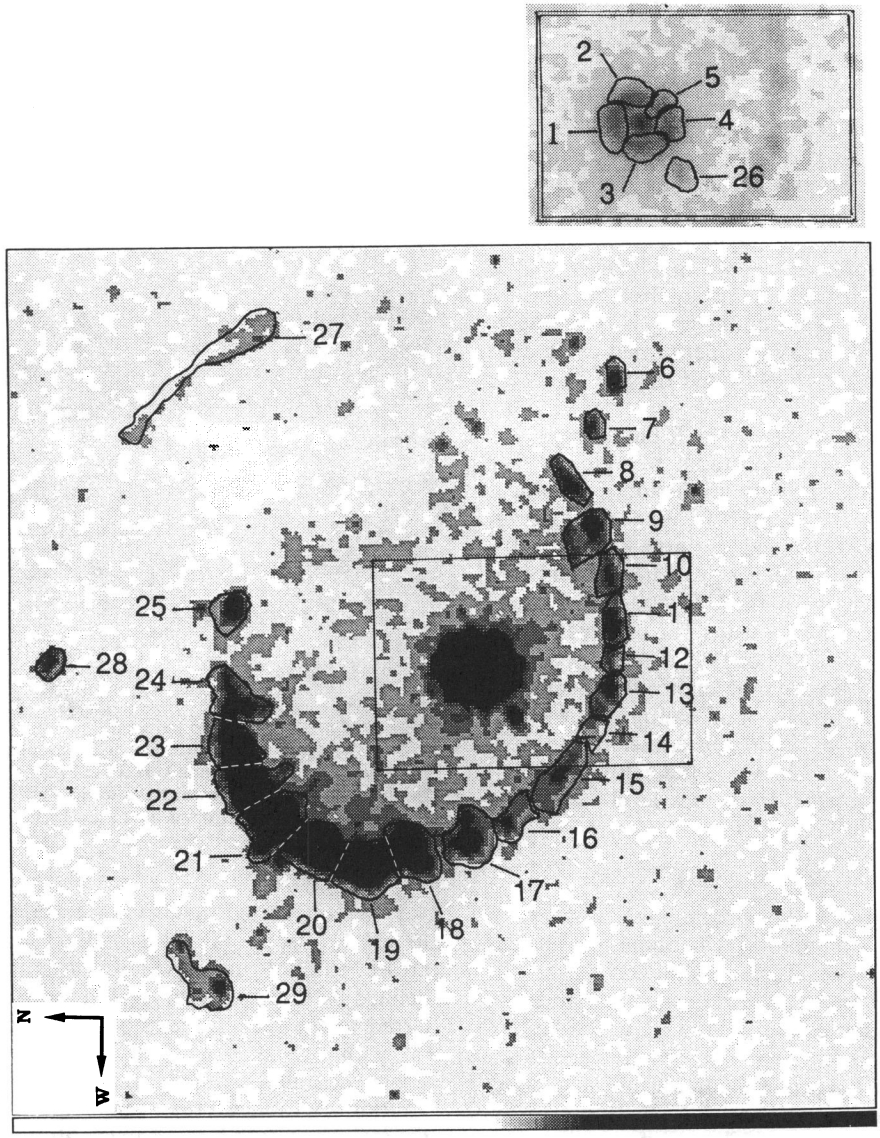

FIG. 2.—Gray-scale image of Arp 10 through a narrow band (80 Å wide) filter centered close to the wavelength of redshifted Hα and [N II]. The inset shows the same region defined by the box but at a different gray-scale contrast level, emphasizing the ringlike nature of the inner ring. The numbered regions are discussed in the text.

inner ring which also exceeds the isophotal limit over its entire extent. The two western knots associated with the ring-arc at a surface-brightness level of 0.3×10^{-16} ergs s^{-1} cm^{-2}. Although this was below our isophotal limit, we decided to include the arc region for completeness.

The regions used in the constant aperture method (Method II) a–s, are presented in Table 2. The circular aperture was centered at each bright knot which was included in the regions selected for Method I. In this way the regions a–f correspond roughly to regions 6–11 and regions g–s to regions 13–25.

Star-formation rates have been estimated from Hα fluxes by a number of authors but most notably by Kennicutt (1983) and Gallagher, Hunter, & Tutukov (1984, hereafter GHT). The assumptions in either case are similar. It is usually assumed that the Hα emission arises from Case B hydrogen recombination in balance with a strong ionizing continuum dominated by stars in the 30 to 60 $M_\odot$ range. Observationally, the Hα flux can be converted to the number of Lyman continuum photons through the expression

$$N_c = 8.78 \times 10^{61} F_c(\mathrm{H}\alpha) D^2 , \quad (1)$$

where D is the distance to the galaxy in Mpc, and $F_c(\mathrm{H}\alpha)$ is the Hα flux in units of ergs s^{-1} cm^{-2} corrected for reddening. In order to derive from this a SFR it is usual to assume a fixed slope for the IMF and an upper mass cutoff. If these factors do not change from region to region in a galaxy and if, additionally, there are few or no super-massive stars present in the H II regions (e.g., Wolf-Rayet stars), then changes in Hα flux are attributed to changes in the total number of stars born per year. For example, GHT estimate that for a Salpeter IMF for the form $\Phi(M) = M^{-a}$ with $a = 2.35$ and $M_{\mathrm{upper}} = 100\ M_\odot$, the SFR is

$$\alpha_c = 2.5 \times 10^{-54} N_c \text{ stars yr}^{-1} . \quad (2)$$

Virtually all the ionizing photons are produced by 30–60 $M_\odot$ stars with lifetimes 3×10^6 yr; so formally α_c provides an

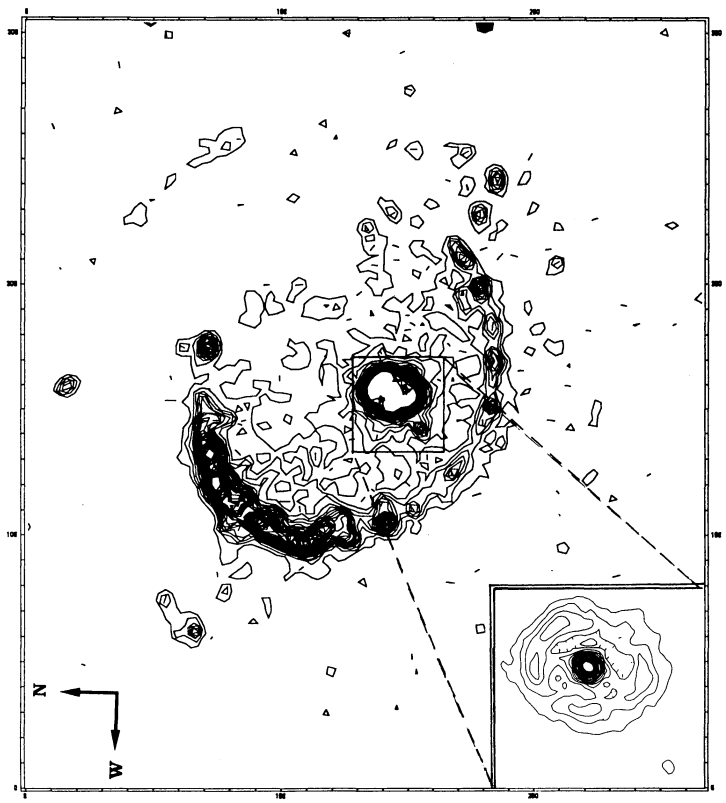

FIG. 3.—Contour map of Figure 2. The contour levels are at 0.36×10^{-16} ergs cm^{-2} arcsec^{-2} increments, between 0.36×10^{-16} ergs cm^{-2} arcsec^{-2} and 14.3×10^{-16} ergs cm^{-2} arcsec^{-2}. The inset shows details of the inner ring and nucleus.

instantaneous value for the SFR. Integrating over the mass range 10–100 $M_\odot$, it is easy to show that this corresponds to a SFR, measured in gas mass converted into massive ($M > 10$ $M_\odot$) stars per year, of $0.7\alpha_c$ $M_\odot$ yr^{-1}. If all stars are included down to a lower mass cutoff of 0.1 $M_\odot$ the total SFR would equal $5.8\alpha_c$ $M_\odot$ yr^{-1}. This agrees closely with the estimate by Kennicutt (1983) adopting very similar assumptions.

5. RESULTS

The results of Method I are presented in Table 1. Column (1) gives the name of the region identified in Figure 2, and column (2) presents the area of the region in arcsec^2. In columns (3) and (4) we show the magnitude of the region measured through the Hα and *R*-band filters, respectively (see § 2). In column (5) we give the Hα surface brightness, after applying a correction for an assumed 5% contamination of the Hα flux by [N II] emission. Such a correction is consistent with the work of Kennicutt (1983) on irregular galaxies and is similar to that measured in the Cartwheel ring galaxy by Fosbury & Hawarden (1977). In column (6) we present the *R*-band surface brightness of each region. Both columns (5) and (6) have also been corrected for a Galactic extinction of $A_v = 0.15$ (de Vaucouleurs et al. 1976). In column (7) we show the luminosity of each region, and finally in column (8) we present the SFR in units of stars Gyr^{-1} pc^{-2}. We note that no correction has been made for internal extinction within the galaxy itself.

In Table 2 we present the results of Method II. Column (1) indicates the region identified in Figure 2, column (2) presents the constant area in arcsec^2, and the columns (3) to (6) have similar information to that of Table 1.

The luminosities of the H II region complexes (see Table 1) show a wide spread in values, ranging from approximately 3×10^{39} ergs s^{-1} in the outer ring-arc (region 27) to 2×10^{40} ergs sec^{-1} in the inner ring (region 2). Although the regions we have evaluated probably contain more than one individual H II region (this is especially true in the bright northwestern regions of Ring 2), it is interesting to note that in all cases the luminosities are comparable with the brightest H II regions seen in late-type galaxies (Kennicutt 1988). For example, even the emission from knot 28 in the outer ring-arc has the luminosity of an average H II region observed in an Sbc or Sc galaxy.

6. MODEL PREDICTIONS FOR RING GALAXIES

It was demonstrated by Toomre (1978) that mildly off-center collisions between galaxies drive ringlike waves through their disks. This work was extended by ASM and SMA to include the study of the star-formation response in ring galaxies. This showed that the overdensity in the ring can be used as a probe of the sensitivity of the star-formation rate to the density in the ring wave. Indeed, mildly off-center collisions are shown to lead to a strong azimuthal variation in ring gas density. In Figure 4*a* we show the density distribution of an expanding ring wave driven into a disk derived from Figure 7*c* of ASM. We have modified the figure to include a notation which will allow us to discuss further the azimuthal dependence of the star formation rate on the ring density, using the letters A to F to indicate azimuth angles around the ring at intervals of 60 degrees. The dependence of the predicted star-formation rate on the ring density (relative to the unperturbed density) is shown for two forms of star-formation rate law. The first,

TABLE 1

PHOTOMETRY OF Arp 10 USING THE CONSTANT ISOPHOTAL LEVEL METHOD

Region[a] (1)	Area (arcsec^2) (2)	$m_{H\alpha}$ (mag) (3)	m_R (mag) (4)	$\sigma_{H\alpha}$[b] ($\times 10^{-16}$ ergs s^{-1} cm^{-2} arcsec^{-2}) (5)	σ_R (mag arcsec^{-2}) (6)	L ($\times 10^{39}$ ergs s^{-1}) (7)	SFR (stars Gyr^{-1} pc^{-2}) (8)
1	4.10	18.38	17.32	23.57	18.66	17.23	22.03
2	4.86	18.16	17.07	24.40	18.59	21.10	22.80
3	4.13	18.6	17.3	19.09	18.64	14.07	17.84
4	4.30	18.46	17.25	20.90	18.64	16.01	19.53
5	2.79	19.24	17.77	15.66	18.69	7.80	14.63
6	5.31	20.59	20.82	2.37	22.44	2.25	2.22
7	4.31	20.9	20.78	2.20	22.17	1.69	2.06
8	9.43	19.91	19.52	2.50	21.76	4.21	2.34
9	18.35	19.02	18.28	2.92	21.24	9.56	2.73
10	11.40	19.91	18.8	2.07	21.25	4.21	1.94
11	12.58	19.64	18.8	2.40	21.35	5.40	2.25
12	7.58	20.55	19.39	1.72	21.40	2.34	1.62
13	12.61	19.73	18.86	2.21	21.41	4.97	2.07
14	8.369	20.87	19.31	1.16	21.42	1.74	1.09
15	17.07	19.54	18.47	1.94	21.35	5.92	1.82
16	16.51	19.78	18.75	1.61	21.60	4.75	1.51
17	22.75	18.59	18.24	3.50	21.44	14.20	3.27
18	38.10	18.3	17.93	2.73	21.69	18.55	2.56
19	28.99	17.68	17.64	6.35	21.10	32.83	5.94
20	31.90	17.71	17.63	5.62	21.19	31.93	5.25
21	27.92	17.96	17.94	5.10	21.36	25.37	4.77
22	24.26	17.73	17.96	7.25	21.22	31.36	6.78
23	23.73	17.83	18.01	6.76	21.25	28.60	6.32
24	19.16	18.99	18.4	2.87	21.41	9.82	2.69
25	17.73	19.23	19.25	2.49	22.17	7.87	2.33
26[c]	10.49	19.94	17.43	2.19	19.79	4.09	2.05
27	112.30	18.81	19.55	0.57	24.48	11.60	0.54
28	21.24	20.12	21.94	0.91	25.06	3.47	0.86
29	67.66	19.1	20.98	0.73	25.36	8.88	0.69
30[d]	114.44	15.82	14.26	8.93	19.21	182.11	8.35
31[e]	575.91	15.32	14.8	2.81	21.50	288.62	2.63

[a] Regions 1–5 correspond to Ring 1, regions 6–25 to Ring 2, and regions 27–29 to Ring 3.
[b] It is $\sigma_{H\alpha} = [F_c(H\alpha)]$/area, where $F_c(H\alpha) = f_\nu \Delta_\nu$, corrected for 5% [N II] emission, $f_\nu = 10^{-(m_{H\alpha}+48.6)/2.5}$ and $\Delta_\nu = 5.26 \times 10^{12}$ Hz.
[c] This is the extra-nuclear knot.
[d] This area corresponds to the integrated values for Ring 1.
[e] This area corresponds to the integrated values for Ring 2.

TABLE 2

PHOTOMETRY OF RING 2, USING THE CONSTANT APERTURE METHOD

Region[a] (1)	Area (2)	$m_{H\alpha}$ (3)	m_R (4)	$\sigma_{H\alpha}$ ($\times 10^{-16}$ ergs s^{-1} cm^{-2} arcsec^{-2}) (5)	σ_R (mag arcsec^{-2}) (6)
a	25.87	20.48	20.70	1.54	22.89
b	25.87	20.67	20.26	1.28	22.46
c	25.87	19.16	19.67	5.18	21.87
d	25.87	19.56	19.21	3.59	21.41
e	25.87	20.33	19.05	1.77	21.25
f	25.87	20.05	19.23	2.29	21.43
g	25.87	20.10	19.27	2.18	21.47
h	25.87	21.00	19.32	0.95	21.52
i	25.87	20.25	19.17	1.89	21.36
j	25.87	20.40	19.48	1.65	21.68
k	25.87	19.07	19.15	5.66	21.35
l	25.87	19.45	19.21	3.97	21.41
m	25.87	18.42	18.68	10.27	20.88
n	25.87	18.64	18.88	8.37	21.07
o	25.87	18.64	18.89	8.38	21.08
p	25.87	19.23	18.85	12.23	21.05
q	25.87	18.27	18.77	11.76	20.97
r	25.87	19.85	19.07	2.75	21.27
s	25.87	19.62	19.99	3.40	22.19

[a] There is a direct correspondence between the regions used in this method, Method II, and those used in Method I (presented in Table 1). The regions a–f correspond roughly to regions 6–11 and regions g–s to regions 13–25 (see § 4)

Figure 4*b*, is derived directly from ASM Model E and as discussed in that paper, follows approximately a Schmidt law in which the SFR $\propto \rho^{1.5}$. The second law, hereafter called the "threshold" model, has a SFR which follows a Schmidt law below some critical gas surface density, but then increases rapidly above that density (see Fig. 4*c*). Using the lettering system defined in Figure 4*a* to identify azimuthal position of the region around the ring, it is noted that both star-formation laws exhibits systematic behavior with azimuth. In the case of the Schmidt law model, the behavior in the SFR/density domain is a loop which begins at the left of the diagram (Position A in Fig. 4*a*; low density, small star-formation rate), rises monotonically through the densest part of the wave (B through D) and then falls back to its initial value in the least dense part of the ring (E through F). In the case of the threshold model, similar behavior is found until the threshold is exceed, where the SFR follows a much steeper path, again forming a tight loop. The threshold model of Figure 4*c* shows some important differences from the Schmidt-type model for Figure 4*b*. Firstly, the SFR/density relationship shows a sudden discontinuity at the critical density. This would have direct observational consequences if star-formation rates and ring densities could be determined over a wide enough dynamic range on either side of the discontinuity. Secondly, because of the peculiar geometry of the off-center collision shown here, the sudden steepening of the SFR law at the criti-

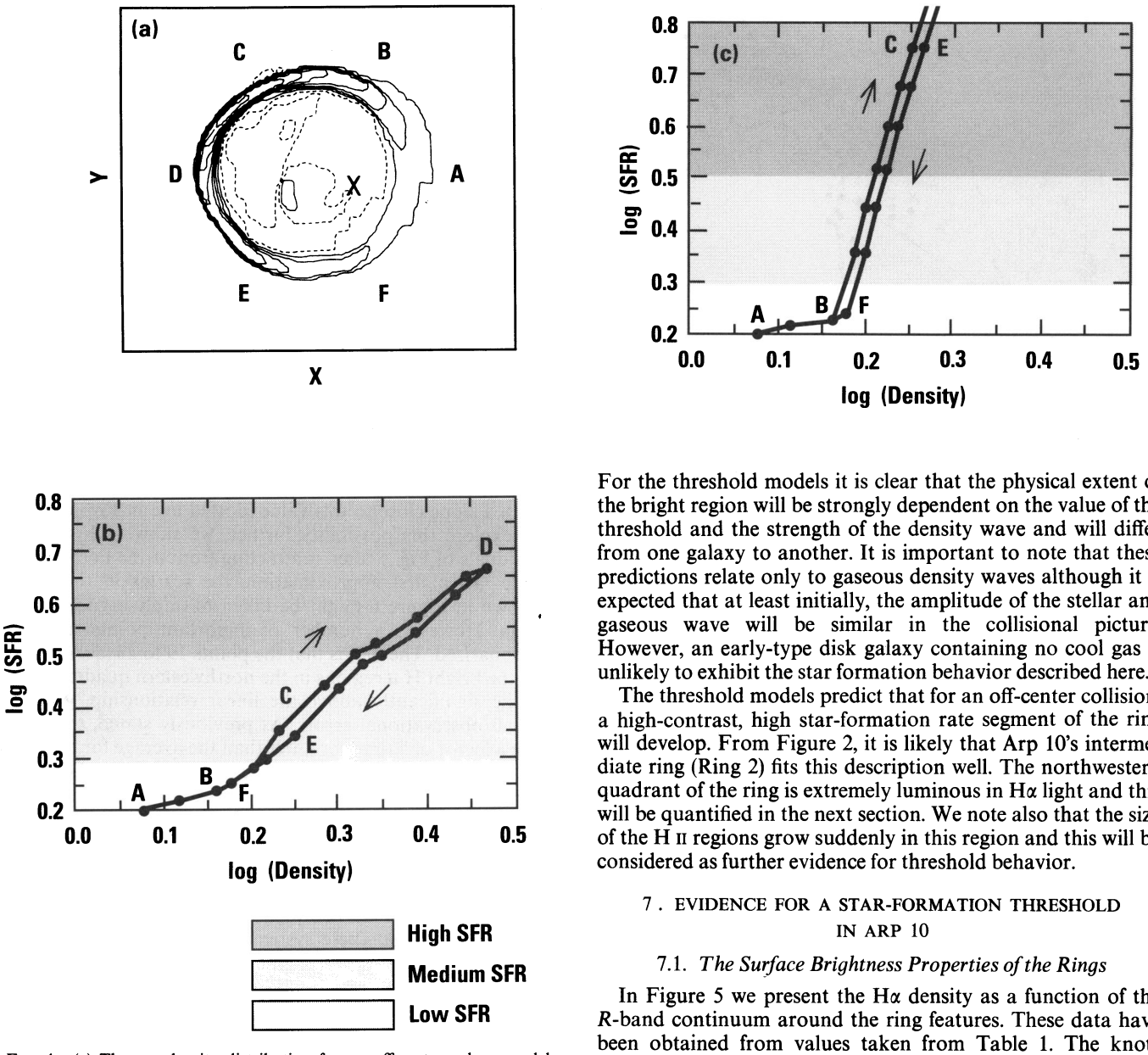

FIG. 4.—(*a*) The gas density distribution for an off-center galaxy model (Model E) from the work of Appleton & Struck-Marcell (1987). Note that the density varies with azimuth around the ring. We have labeled azimuthal positions around the ring with the letters A to F for reference. (*b*) The relationship between the star-formation rate (SFR) and gas density for the model shown in (*a*). The behavior follows that of a Schmidt law (see text). The letters refer to the azimuthal positions given in (*a*). (*c*) The same relationship as in (*b*) but for a "threshold" star-formation law. Here the SFR follows a Schmidt law below a critical density (In this case 1.5 × the unperturbed density) and then changes to a steeper form in which SFR $\propto \rho^6$ above the critical density.

cal density translates into a sudden brightening of the ring in Hα light in an arc encompassing the densest parts of the ring. For example, in Figure 4*c*, the azimuthal regions of the ring extending between points C and E in Figure 4*a*, lie well above threshold and would be emitting strongly at the wavelength of Hα. (We note that point D is so luminous in this model it lies outside the range of the plotted points in Fig. 4*c*.) In contrast, from Figure 4*b*, it can be seen that only a small region near point D would be expected to be producing stars at a high rate. For the threshold models it is clear that the physical extent of the bright region will be strongly dependent on the value of the threshold and the strength of the density wave and will differ from one galaxy to another. It is important to note that these predictions relate only to gaseous density waves although it is expected that at least initially, the amplitude of the stellar and gaseous wave will be similar in the collisional picture. However, an early-type disk galaxy containing no cool gas is unlikely to exhibit the star formation behavior described here.

The threshold models predict that for an off-center collision, a high-contrast, high star-formation rate segment of the ring will develop. From Figure 2, it is likely that Arp 10's intermediate ring (Ring 2) fits this description well. The northwestern quadrant of the ring is extremely luminous in Hα light and this will be quantified in the next section. We note also that the size of the H II regions grow suddenly in this region and this will be considered as further evidence for threshold behavior.

7. EVIDENCE FOR A STAR-FORMATION THRESHOLD IN ARP 10

7.1. *The Surface Brightness Properties of the Rings*

In Figure 5 we present the Hα density as a function of the *R*-band continuum around the ring features. These data have been obtained from values taken from Table 1. The knots associated with the three ring structures are indicated. As one proceeds from Ring-arc 3 (outer ring-arc) to the slightly higher *R*-band surface brightness levels, σ_R, in Ring 2, the Hα surface brightness increases slowly with an average value of approximately 3.1×10^{-22} ergs s^{-1} cm^{-2} pc^{-2}. However, as one proceeds to higher levels of σ_R, an increase in scatter of the points is observed near $\sigma_R = 21.3 \pm 0.2$ mag $arsec^{-2}$. Although some of the scatter is attributable to measurement error (especially region 14), most of the scatter is due to regions 19 through 23, which are significantly more luminous (by a factor of 5 on a linear scale) in Hα light than the other regions with similar σ_R. These points correspond to the bright regions of the ring noted by Vorontsov-Velyaminov. Finally, we proceed to Ring 1 (the inner ring). Here the Hα surface brightness is well determined but the strength of the red continuum is only poorly known. This is because the ring is embedded in a strong central bulge which dominates the red light. We therefore accounted for the bulge contribution to the light by fitting an $R^{1/4}$ law profile to the bulge and then removing its contri-

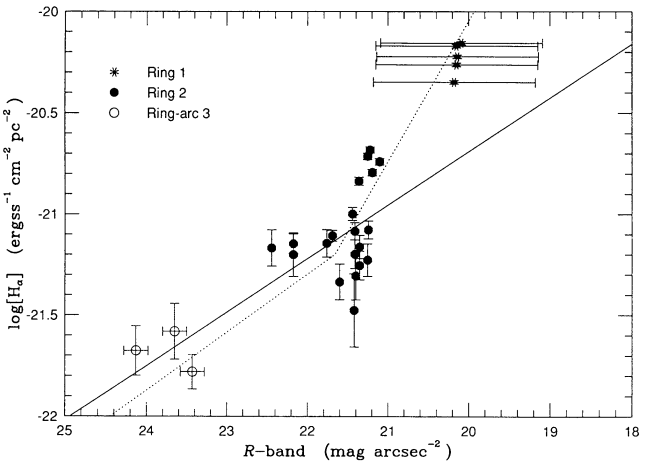

FIG. 5.—Plot of Hα vs. *R*-band surface brightness for the constant isophote method (see § 4, Table 1). The different symbols indicate data for the three ring structures. Note that the large error bars for Ring 1 indicate our uncertainty in the removal of the bulge light which dominates the *R*-band emission for the inner ring. The solid line shows a linear-fit to these data and the dotted lines show the result of a two-line fit (see text).

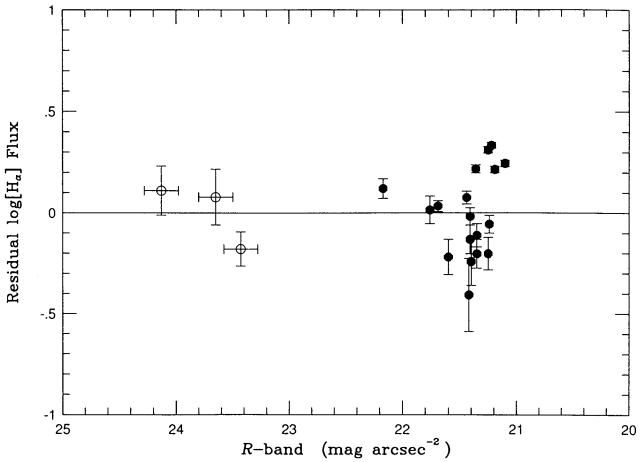

FIG. 6.—Plot of the residuals from Fig. 5 after the subtraction of the linear fit through the points of Ring 2 and Ring-arc 3.

bution to the inner ring. Because of uncertainties in the fit to the bulge light, the surface brightness at *R*-band for the Ring 1 points have correspondingly large errors (see Fig. 5). However, they do provide an important extra piece of evidence for a threshold star-formation law in Arp 10 as discussed below and so we have included them for completeness in Figure 5.

As discussed in § 4, we repeated the surface brightness estimates for the Ring 2 using the constant aperture method (Method II). We confirmed that an increase in dispersion was observed in the Hα surface brightness at a level of 21.3 mag arcsec^{-2}, in accord with the earlier result of Figure 5.

7.2. *The Possible Contamination of the R-band Light by Young Stars*

Before proceeding to discuss the implications of Figure 5 for testing models of density wave induced star formation, we must first question the assumption that the red continuum light is dominated by old stars in the ring waves, rather than light from young star clusters. We have already noted that the distribution of *R*-band emission in the rings is rather smooth relative to that of the Hα emission and this fact alone argues that our continuum measurements are not strongly influenced by light from young stars. However, for the purposes of the following discussion we will adopt a "worst-case contamination" approach to the problem and assume that all of the red continuum light results from emission from underlying young stars and explore its impact on our conclusions.

If the underlying young clusters dominate the red continuum then this is likely to lead to a correlation between log [F(Hα)] and a broad-band continuum magnitude. Such a loose correlation is observed in studies of H II regions in late type galaxies (see Kennicutt & Chu 1988). The correlation can be understood in terms of a set of self-similar clusters of increasing size in which the ratio of the Hα to continuum flux remains fixed. Assuming that all other properties of the cluster remain the same (age, metallicity, IMF) then such a set of clusters would lead to a linear correlation between log [F(Hα)] and σ_R with a slope of -0.4. Indeed we note that formally fitting a straight line to the data for Ring 2 and Ring-arc 3 yields a line with a slope close to this value (dotted line in Fig. 5). In order to explore this possibility further, we show in Figure 6, the residuals of Fig. 5 after subtracting from it the linear fit to the data. To a first approximation, the scatter in the residuals shown in Figure 6 might be taken to imply a good fit to the data. However, a number of important points need to be emphasized. The first is that the points 19 to 23 (corresponding to the bright H II regions in the northwestern quadrant of Ring 2) lie significantly above the linear relationship, given their small observational errors. As previously stated, these points are a factor of 5 times brighter than the average for their values of σ_R. Secondly, we will show conclusively in § 7.4, that the apparent scatter in the residuals shown in Figure 6 for Ring 2, especially near $\sigma_R = 21.3 \pm 0.2$ mag arcsec^{-2}, arises from *systematic azimuthal changes* around the ring, not random errors in the linear relationship. This subtle point is crucial to our later argument about the nature of the enhancement of emission in the northwestern quadrant of Ring 2. We will demonstrate below, that these systematic variations away from the linear fit are naturally explained within the context of the threshold star formation model. However, as the linear fit to Figure 5 may imply, we cannot rule out some contamination by young stars as an explanation for the increase in red light in the brighter Hα emitting regions. Even if some degree of contamination does exist from young stars, it does not invalidate the main conclusion, that the H II regions observed in regions 19–23 of Figure 2 are unusually bright as compared with other H II regions with the same *R*-band continuum.[2]

7.3. *Density Wave Induced Star Formation*

Another equally valid way of interpreting Figure 5 is to assume that Arp 10 is a collisional ring galaxy in which density waves are driven through its disk. The slow decline in σ_R as one

[2] Another approach to the question of contamination of the *R*-band flux from the underlying host cluster would have been to predict the expected contribution to the *R*-band emission based on the strength of the Hα flux. In order to do this we would have had to assume values for the IMF, the metallicity and the age of the clusters and use a color evolution model to predict the expected *R*-band continuum. We believe that although such models exist for solar abundances, the reliability of such models, especially the treatment of the giant and supergiant stars is still quite questionable. We therefore preferred to make use of the rough correlation derived from observations.

proceeds from inner Ring 1 radially outward to the outer rings would be explained as a consequence of the decreasing strength of the density waves with radius. If we further assume that the stellar ring density can be used to measure the gas density in the expanding wave (see § 7.6), then Figure 5 can be used as a diagnostic of the various forms of star-formation law discussed in § 6. For example, deviations from a simple linear relation in Figure 5, can be interpreted as deviations from a Schmidt law behavior. We have already pointed out in § 7.2, that systematic deviations of this kind do exist. We will now investigate the possibility that these deviations are evidence for a threshold star-formation picture.

The evidence for a SFR threshold law in Arp 10 depends on two things. The first is our ability to recognize a discontinuity in the SFR versus ring density relationship consistent with our model predictions and the second is that such a discontinuity should exhibit the azimuthal variations predicted for the off-center collisional model. As was stated earlier, the former problem is one of dynamic range. Within any one ring, the dynamic range in the star-formation rate is relatively small, despite the apparently bright regions in Ring 2 discussed earlier. Arp 10 provides a useful probe of star-formation mechanisms because its three rings sample a wide range of densities, from the weak outer Ring-arc 3 to the more overdense inner rings.

One simple method of finding a sudden discontinuity in the data similar to that of Figure 4*c* is to split the data presented in Figure 5 into two equal sets ordered by the Hα flux and independently fit a straight line to them. As long as the discontinuity lies somewhere near the center of gravity of the data then two lines of markedly different slope would be found. On the other hand, if the same slope is found for both lines, then this would argue for a continuous function of Hα emission with continuum light. In Figure 5 we show the result of fitting two straight lines to the data for all three rings using a Gauss-Markov elimination method. The method depends critically on good sampling of points on either side of the discontinuity. The only restriction to the fitting procedure was that the crossing point of the two lines should occur somewhere within the body of these data. Despite the very uncertain values for σ_R in Ring 1 (giving these points lower weight), there is evidence for a discontinuous form to the data presented in Figure 5 since the fitted lines do have different slopes. The intersection between the two lines occurs at around $\sigma_R = 21.2$ mag arcsec^{-2} which is similar to the surface density at which the increase in dispersion was noted in the Ring 2 emission alone. As long as it is valid to treat all three rings together, the evidence suggests a threshold star-formation law similar to that discussed in § 6.

The increase in Hα surface brightness at the *R*-band threshold of 21.3 ± 0.2 mag arcsec^{-2} is most easily interpreted as a threshold in the massive SFR. Using the values for the knots presented in Table 1, we plot, in Figure 7, the SFR per square parsec as a function of the red continuum surface density. The discontinuity in Hα surface brightness translates, under these assumptions, into a sudden change in SFR. The rates change from an average of 0.5–1.5 stars Gyr^{-1} pc^{-2} (or 2.9–8.7 $M_\odot$ Gyr^{-1} pc^{-2}) in the fainter outer ring-arc and the faint southern sections of Ring 2 to values which rise to 2–6 stars Gyr^{-1} pc^{-2} (or 11–30 $M_\odot$ Gyr^{-1} pc^{-2}) in the bright northwest portion of Ring 2. Higher star-formation rates of approximately 20 stars Gyr^{-1} pc^{-2} (or 116 $M_\odot$ Gyr^{-1} pc^{-2}) are found for Ring 1. We compare these values with Caldwell et al. (1991) who found rates of less than 0.4 $M_\odot$ Gyr^{-1} pc^{-2} for early-type spirals and values of 4–20 $M_\odot$ Gyr^{-1} pc^{-2} for Sc type galaxies. The local SFR in the inner ring appears to be extremely large, while those in Ring 2 appear to be similar to local SFR of Sc galaxies.

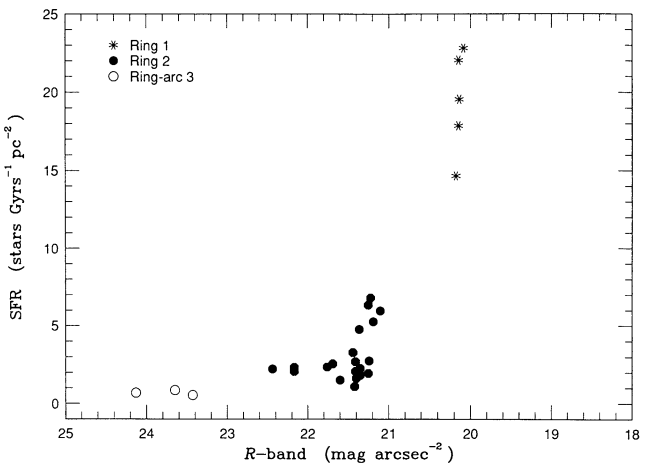

FIG. 7.—Plot of the SFR in the three ring structures, in units of stars Gyr^{-1} pc^{-2}, vs. the *R*-band surface brightness for the constant isophotes method (see § 4, Table 1). Note that the uncertainties in the Ring 1 points are identical to those shown in Fig. 6.

7.4. *Azimuthal Variations in Ring 2*

Much of the foregoing argument for a threshold dependence of star-formation rate on ring strength is based on the assumption that all three rings are generated by a similar dynamical process. However, if Ring 1 was formed, for example, at an inner Lindblad resonance by some other process, then our argument for a threshold star-formation law would be weakened. Nevertheless, there is evidence in Ring 2 alone, for threshold behavior. We have already discussed in § 7.2 the unusually bright star forming complexes in the northwestern quadrant of Ring 2. We will now show that the azimuthal variations in the strength of the star formation is very similar to that expected from the models of Figure 4. In Figure 8 we show an enlarged version of the Ring 2 data presented in Figure 7. Unlike the earlier figure, Figure 8 connects the points with increasing azimuth. The number associated with each point represents the knot number identified in Figure 2. It is clear from Figure 8, that a strong azimuthal trend is evident as the star-formation rate increases in the northwestern quadrant and these data resemble the results predicted in Figure 4*c*. This systematic behavior in the star-formation rate as a function of azimuth provides a good indication that the star-formation rate is being controlled by a global phenomenon and is not a stochastic process. This confirms our earlier statement that the deviations of the H II regions 19–23 from the linear correlation shown in Figure 5 are inconsistent with a random noise process.

7.5. *The Size of the* H II *Regions*

There is an independent piece of evidence that a threshold process may have changed the nature of the star formation in the overdense region of the ring. In a study of H II regions in galaxies of various Hubble types, Kennicut (1988) and Strobel, Hodge, & Kennicutt (1991) demonstrated that there was a well defined relationship between the size of an extra-galactic H II

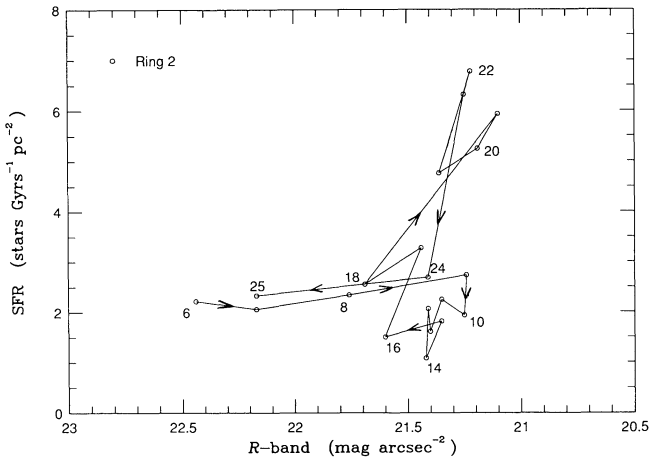

FIG. 8.—Azimuthal behavior of the SFR and R-band continuum for Ring 2. The numbers refer to the Hα emitting regions identified in Fig. 2 and increase numerically as a function of increasing position angle around the ring. We observe the striking similarity with the threshold model shown in Fig. 4*c*.

region and its luminosity in the Hα line. Kennicutt chose to define the "characteristic size" of an H II region in an external galaxy as the diameter of the Hα emission contour defined by the level 2×10^{-16} ergs s^{-1} cm^{-2} arcsec^{-2}. It was shown that the size increased monotonically with the flux from the H II regions in approximate accord with simple arguments concerning the size of the Strömgren sphere. In Figure 9, we show a contour map of the Hα emission at the level of 2×10^{-16} ergs s^{-1} cm^{-2} arcsec^{-2}. What is striking about the map is that the majority of the H II regions which lie below the "threshold" value of R-band flux (Knots 6–16 in Fig. 2) have angular sizes which are barely or just resolved on at the level of a few arcsec. However, as one approaches the northwestern segment of the Ring 2, the H II regions suddenly grow in size until they merge together to form one continuous structure which includes most of the very active parts of the second ring and all of the first ring. It appears that on the basis of the size of the H II regions alone, there is evidence for some form of transition from small to large H II regions which is consistent with our photometric result. Both observational facts indicate that a threshold star-forming process is operating in the galaxy.

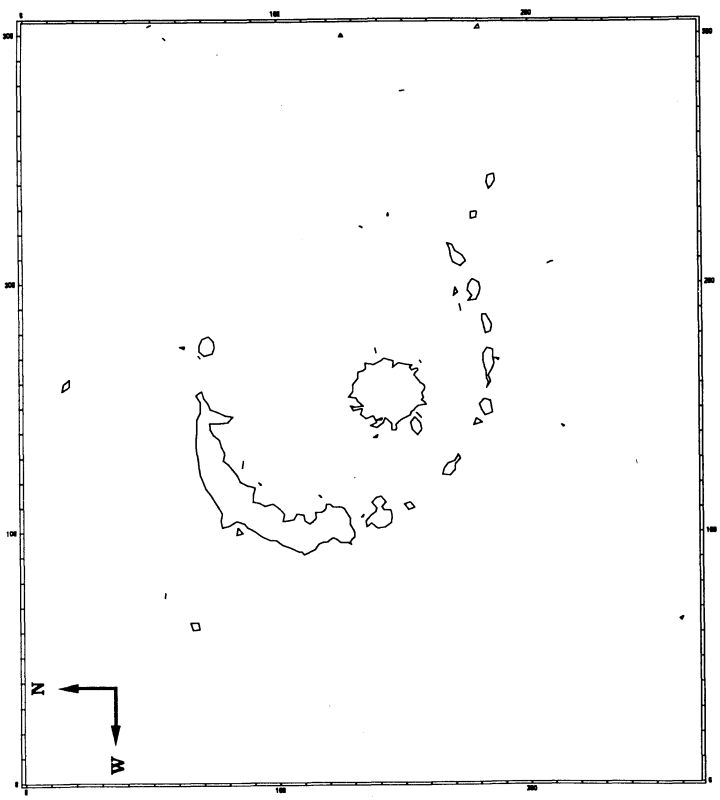

FIG. 9.—Contour map of the Hα emission at the level of 2×10^{-16} ergs cm^{-2} arcsec^{-2}. This isophotal level was used by Kennicutt (1988) to define the "characteristic size" of an H II region. Note that the H II region complexes suddenly grow in size in the bright (northwest) region of Ring 2.

7.6. *Consequences for Other Star-Formation Threshold Models*

We have presented evidence that suggests that the amplitude of the stellar density wave in Ring 2 is a controlling influence in the processes of star formation in the ring. At some critical (threshold) surface density in the red starlight, a change occurs in the properties of the H II regions. The changes are consistent with a sudden increase in star-formation rate. We will now discuss possible way in which such changes may come about in the context of models of star formation in external galaxies.

Kennicutt (1989) has presented convincing evidence for a star-formation threshold in a sample of normal disk galaxies. By combining information about the total gas surface density derived from CO and H I measurements, Kennicutt was able to demonstrate that massive star formation ($M > 10\ M_{\odot}$) occurs mainly in regions of the disk which lie above a critical gas surface density. The form for the critical density follows from a stability analysis of a thin self-gravitating disk applied to the gaseous component (Toomre 1964; Goldreich & Lynden-Bell 1965). Kennicutt found that in regions above the gas density threshold, the star-formation law followed a Schmidt type form (SFR $\propto \rho^n$ with $n \simeq 1.3$), whereas below the threshold, little or no massive stars were being formed.

Firstly, we point out that our observations of Arp 10 cannot be directly compared with the work of Kennicutt unless we make some assumptions about the nature of the rings. We do not yet have information about the distribution of H I or CO observations in this galaxy and therefore we cannot directly compare the star-formation rates in the rings to the gas surface densities. However, we can appeal to our theoretical understanding of the ring galaxy phenomenon to help restrict the range of possibilities.

If Arp 10 is a colliding ring galaxy, then the stellar surface density in the ring will be a lower limit to the surface density in the gas component. For example, in the absence of self-gravity in the gas, the density profile of the expanding ring perturbation would closely track that of the stars since both gas and stars are crowded into the density wave (see SMA). In this simplified case, a measurement of the old stellar surface density would be equivalent to a measurement of the gas surface density in the ring. Even in the case where hydrodynamic effects begin to dominate in the gas phase, the strength of the stellar density wave will provide a lower limit to the density in the gas. In general, whereas the gas will tend to occupy a smaller volume than the old disk stars in the wave, the inverse is unlikely to be true.

Since we do observe H II regions in all three rings we conclude that the rings must have already exceeded Kennicutt's critical density over most of their area. However, the marked increase of the Hα flux in the northwest quadrant of Ring 2

suggests that in colliding systems the star-forming behavior is more complicated. In particular, the existence of a threshold that depends on the strength of the density wave may provide evidence for a breakdown of the linear instability model which appears to provide a good description of star formation in isolated galaxies. This may not be surprising, since strong gravitational interactions and collisions are expected to drive highly nonlinear behavior in galaxies.

7.7. *Global Star-Formation Rate in Arp 10*

Under the same assumption as in § 7.1, we can calculate the total SFR in the galaxy, including the two rings, the ring-arc and the nuclear emission. The resulting SFR is approximately 0.94 stars yr^{-1} (or 5.4 $M_\odot$ yr^{-1}). Compared with a typical late-type galaxy, this overall SFR is at the low end of the distribution (GHT; Caldwell et al. 1991). This contrasts with the high local SFR within the rings themselves. The apparent paradox is a result of the narrowness of the rings. In comparison, a typical Sc galaxy would have H II regions of similar luminosity to Arp 10, but would be distributed over a larger area of the disk.

7.8. *IMF Variations?*

There is another way we can interpret the elevated Hα fluxes in the overdense regions without invoking a change in the star-formation rate. An equally plausible way of increasing the number of Lyman continuum photons in the "active" regions would be to modify the IMF in those regions. Since the number of Lyman continuum photons N_c in all H II regions is mainly produced by stars in the 30 to 60 $M_\odot$ region, small changes in the slope of the IMF can lead to quite large differences in the N_c. For example in order to increase N_c (and therefore by implication $\sigma_{H\alpha}$) by a factor of 4–5 one only has to flatten the slope of the IMF from a value of 2.35 to 1.95 (assuming an upper mass cutoff of 100 $M_\odot$). This is sufficient to explain the sudden increase in the Hα emission in the overdense regions of Ring 2. However, if the same process is to give rise to much brighter fluxes seen in the inner ring, the slope would have to be modified substantially from 2.35 to 1.55. As discussed by Kennicutt (1983), such large changes in the IMF slope would have noticeable consequences for the broad-band colors of star formation regions. Since we do not yet have multicolor images of Arp 10, the possibility that changes in IMF slope can explain the higher Hα fluxes in the overdense regions cannot be ruled out. The slope of the IMF though, is not the only parameter that can produce this result. If the upper mass cutoff is smaller than 60 $M_\odot$, then this has a direct impact to the number of Lyman continuum photons produced. It has been assumed that $M_{upper} = 100\ M_\odot$. However recent observations (Doyon, Puxley, & Joseph 1992) indicate that there are galaxies with $M_{upper} < 40\ M_\odot$. It is not clear that physical mechanism could modify the IMF in the dense parts of the ring-wave.

8. CONCLUSIONS

We have performed CCD imaging of the peculiar galaxy Arp 10 and have drawn the following conclusions from our observations:

1. Arp 10 is shown to contain two massive star-forming rings and an outer star-forming ring-arc indicating that star formation is occurring concurrently on a variety of scales. The morphology of Arp 10 is consistent with that of a colliding ring galaxy. We identify a possible small elliptical companion galaxy which lies on the minor axis of Ring 2, which may be the intruder galaxy.

2. The strength of the Hα emission in the rings covers a wide range of Hα surface brightness, ranging from extremely luminous in the inner ring (comparable to the most luminous H II regions in the late-type spiral galaxies) to rather faint H II regions in the outer ring-arc (comparable to the most luminous H II regions seen in Sa type galaxies).

3. We present evidence for a sudden change in the properties of the ring H II regions as a function of the strength of the underlying stellar density wave. These are

(a) Taking the three ring structures together, there is evidence for a discontinuous relationship between the logarithm of the Hα surface brightness and the strength of the R-band continuum surface density which support a threshold star-formation model. We interpret the sudden increase in Hα emission at a σ_R of 21.3 ± 0.2 mag $arcsec^{-2}$ as either a sudden increase in the SFR or a change in the IMF at a critical matter density in the ring. In either case, the result suggests that the star-formation properties are being controlled by the amplitude of the stellar surface density in the ring.

(b) The proposed critical threshold value in σ_R falls within the range spanned by Ring 2. At this apparent threshold level, the star-formation properties show a large dispersion, due mainly to an increase by a factor of 5 in the star-formation rates in the north-western quadrant of the ring. This is the same quadrant of the ring which was noted as unusual by Vorontsov-Velyaminov (1977). The azimuthal variations of both star-formation rate and R-band light show remarkable similarity with model predictions for off-center ring galaxy in which a threshold star-formation law holds.

(c) The sizes of the H II regions are observed to grow suddenly in the region of the enhanced star formation discussed in (b) above, again supporting the proposed threshold picture.

4. The results indicate that the star formation behavior may differ from that of a normal queiscent disk system as a result of the existence of strong nonlinear waves induced in the disk by a collision. A full comparison with the gas density threshold models of Kennicutt (1989, 1990) will require observations of the cool gas content of the three star-forming rings.

We thank C. Struck-Marcell (Iowa State University) for stimulating discussions and L. Fontaine (Graphic Design, ISU) for advice and help regarding Figure 4. The authors would like to thank J. Eitter (Iowa State University) for invaluable help at all stages of the observations at the Fick Observatory, and G. Aldring (University of Minnesota) for providing the design for the f/4 focal reducer. P. N. A. wishes to thank the Department of Physics and Astronomy for providing travel funds to KPNO. The authors are grateful to an anonymous referee for suggesting some significant improvements to the paper.

APPENDIX

In this section we compare the *R*-band image of Arp 10 taken at KPNO with the one that we took at Fick Observatory, as a further check that it has no contamination by hydrogen emission lines. Since the two images had different resolution we convolved them with a Gaussian profile down to an effective resolution of FWHM = 3.″3. A contour graph of each image is presented in Figures 10 and 11. Our calculations of the intensity distribution along Ring 2 in both images showed that there was no discernible difference between the two, down to a level of less than 5%.

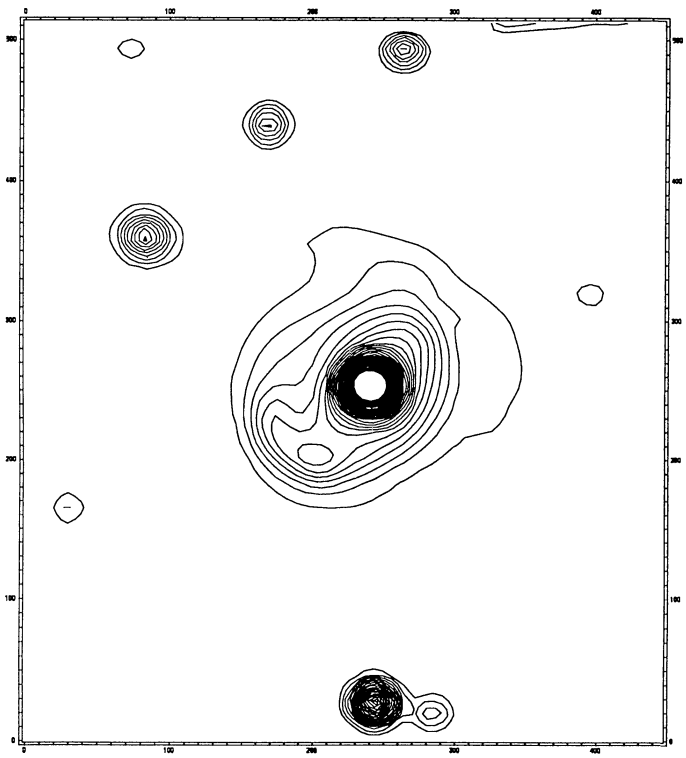

FIG. 10

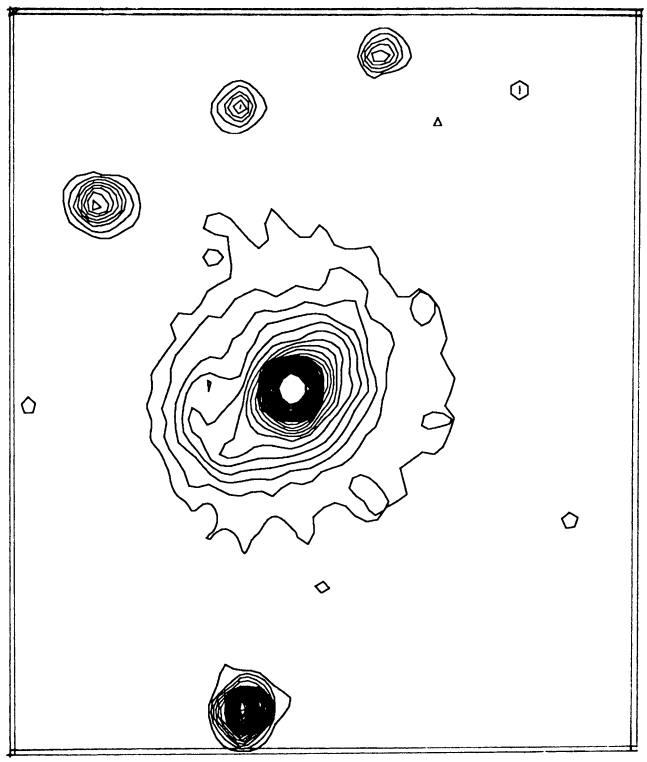

FIG. 11

FIG. 10.—Contour map of the KPNO image presented in Fig. 1 after convolution with a Gaussian profile. The resulting effective resolution is 3.″3 (FWHM).

FIG. 11.—Contour map of the Fick Observatory CCD image obtained through a narrow-band filter. The filter is shifted with respect to Hα emission line and as a result is completely free of any possible line contamination (see text). Note the strong similarities (down to a level of less than 5%) between this image and Fig. 10.

REFERENCES

Appleton, P. N., & Struck-Marcell, C. 1987, ApJ, 312, 382 (ASM)
Arp, H. C. 1966, Atlas of Peculiar Galaxies (Pasadena: Caltech)
Caldwell, N., Kennicutt, R., Phillips, A. C., & Schommer, R. A. 1991, ApJ, 370, 526
Carignan, C., & Beaulieu, S. 1989, ApJ, 347, 760
Dahari, O. 1985, ApJS, 57, 643
de Vaucouleurs, G., de Vaucouleurs, A., & Corwin, H. G., Jr. 1976, Second Reference Catalog of Bright Galaxies (Austin: Univ. Texas Press)
Doyon, R., Puxley, P. J., & Joseph, R. D. 1992, ApJ, 397, 117
Fosbury, R. A. E., & Hawarden, T. G. 1977, MNRAS, 178, 473
Gallagher, J. S., Hunter, D., & Tutukov, A. 1984, ApJ, 284, 544 (GHT)
Goldreich, P., & Lynden-Bell, D. 1965, MNRAS, 130, 97
Kennicutt, R. 1983, ApJ, 272, 54
———. 1988, ApJ, 334, 144
———. 1989, ApJ, 344, 171
———. 1990, in The Interstellar Medium in Galaxies, ed. H. A. Thronson, Jr., & J. M. Shull (Dordrecht: Kluwer), 127
———. 1991, ApJ, 370, 526
Kennicutt, R., & Chu, Y.-H. 1988, AJ, 95, 720
Landolt, A. U. 1983, AJ, 88, 439
Lynds, R., & Toomre, A. 1976, ApJ, 209, 383
Malin, D. F., & Carter, D. 1983, ApJ, 274, 534
Scalo, J. M., & Struck-Marcell, C. 1984, ApJ, 276, 60
———. 1986, ApJ, 301, 77
Schombert, J. M., & Bothun, G. D. 1988, AJ, 95, 1389
Skillman, E. D. 1987, in Star Formation in Galaxies, ed. C. Lonsdale (NASA CP 2466), 267
Stone, R. 1977, ApJ, 218, 767
Struck-Marcell, C. 1990, AJ, 99, 71
Struck-Marcell, C., & Appleton, P. N. 1987, ApJ, 323, 480 (SMA)
Strobel, N. V., Hodge, P., & Kennicutt, R. C. 1991, ApJ, 383, 148
Sulentic, J. W., & Arp, H. 1983, AJ, 88, 489
Theys, J. C., & Spiegel, E. A. 1977, ApJ, 212, 616
Toomre, A. 1964, ApJ, 139, 1217
———. 1978, in IAU Symp. 79, The Large-Scale Structure of the Universe, ed. M. S. Longair & J. Einasto (Dordrecht: Reidel), 109
Vorontsov-Velyaminov, B. A. 1977, Atlas of Interacting Galaxies, A&AS, 28, 1